Characterization of the surface structure of CH_3 and CF_3 terminated *n*-alkanethiol monolayers self assembled on Au{111}

L. Houssiau, M. Graupe, R. Colorado, Jr., H. I. Kim, T. R. Lee, S. S. Perry, and J. W. Rabalais[a)]
Department of Chemistry, University of Houston, Houston, Texas 77204-5641

(Received 6 July 1998; accepted 19 August 1998)

Surface elemental and structural characterization of hexadecanethiol and heptadecanethiol (C_{16} and C_{17} for short) and 16,16,16-trifluorohexadecanethiol (FC_{16}) self-assembled monolayers (SAMs) on a Au{111} surface have been obtained from time-of-flight scattering and recoiling spectrometry. The clean Au surface was also characterized in order to identify the azimuthal orientation of the SAMs with respect to the substrate. Classical ion trajectory simulations were used to relate the experimental scattering and recoiling data to the surface structure. The scattered and recoiled atoms originate from the outermost five–six atomic layers, and azimuthal anisotropy was observed in the measurements. The results provide a model for the SAMs in which the alkyl chains chemisorb with the S atoms situated above the face-centered-cubic (fcc) threefold sites of the Au{111} surface to form a continuous film with a $(\sqrt{3}\times\sqrt{3})R30°$ structure that fully covers the Au surface. The orientation of the molecular axis azimuth of the SAMs relative to the Au azimuthal directions was determined. The data indicate that the molecular chains have specific tilt and twist angles relative to the Au surface and six coexisting domains resulting from the six equivalent tilt directions of the molecular axis. Dramatic changes in the anisotropic patterns of the ion scattering azimuthal scans from the surfaces of the SAMs with different terminations were observed. These phenomena result from the different tilt angles of the CH_3 and CF_3 groups. The data are consistent with free rotation of both the CH_3 and CF_3 groups. The C_{16} SAM exhibited the best azimuthal features and was more resistant to radiation damage from the incident Ar^+ scattering beam than the other films. Due to the tilt angle of the SAMs, an ''ion's eye view'' of the structure, i.e., the positions of the atomic cores as experienced by the incoming keV ions, reveals a regular array of sloping cavities within each unit cell. © *1998 American Institute of Physics.* [S0021-9606(98)70244-2]

I. INTRODUCTION

The chemisorption of organosulfur compounds such as alkanethiols on metal surfaces to form well-defined organic overlayers known as self-assembled monolayers (SAMs) has been an active area of research over the past decade due to the considerable interest of these films for basic research and for technological applications.[1] SAMs are usually prepared on metal substrates by immersion of the substrate into a solution of the adsorbate in an organic solvent such as ethanol. Synthetic methods for preparation of these dense, oriented molecular films have been described.[2] A detailed understanding of the structure, molecular packing, and surface termination of these films is essential for understanding the relationships between microscopic structure and macroscopic chemical and physical properties. An array of experimental analytical techniques, including x-ray photoelectron spectroscopy (XPS),[3] ellipsometry,[4] reflection infrared spectroscopy,[5] transmission electron microscopy[6] (TEM), atomic force microscopy[7–11] (AFM), scanning tunneling microscopy[12–16] (STM), Raman spectroscopy,[17] metastable induced electron spectroscopy[18] (MIES), and low energy electron,[19–21] low energy He atom,[22] and grazing incidence x-ray[23] diffraction, have been used to characterize the structure, order, and bonding of these films. These structures have also been studied theoretically[24–26] using molecular dynamics simulations and quantum mechanical calculations.

The various experimental and theoretical studies referenced above have provided an excellent basis for understanding the structures of SAMs. In this paper, we apply, for the first time, the technique of time-of-flight scattering and recoiling spectrometry[27] (TOF-SARS) to investigate the normal alkanethiols $[CH_3(CH_2)_{n-1}SH]$, where $n=16$ (hexadecanethiol) and 17 (heptadecanethiol), and an alkanethiol with a CF_3 terminal group $[CF_3(CH_2)_{15}SH]$ (16,16,16-trifluorohexadecanethiol), which were deposited on a Au{111} surface. Henceforth, we will refer to these molecules as C_{16}, C_{17}, and FC_{16}, respectively. Analysis of such complex structures is a major challenge for TOF-SARS. Our objective is to take advantage of the novel capabilities of TOF-SARS in order to attempt to answer some of the outstanding questions concerning the structures of the surfaces of SAMs. Some of these questions concern the nature of the chemisorption site of the alkanethiol chains on the {111} metal surfaces, the orientation of the terminal groups at the surface, the degree of free rotation of the terminal groups, the tilt and twist angles of the chains, and the differences in the degree of ordering of even and odd carbon chains of nearly the same chain length.

a)Author to whom correspondence should be addressed.

Here we detail the capabilities of TOF-SARS and its application to structural analyses of organic films. First, the high surface sensitivity of the technique provides information on the outermost layers of the SAMs. It does not probe down to the sulfur-metal interface, which is buried beneath 16 or 17 layers of carbon atoms. In order to identify the chemisorption site of alkanethiols on metal surfaces, we have recently[28] investigated the chemisorption of the simplest prototypical model alkanethiol compound, methanethiol [CH_3SH], on Pt{111} and Au{111} surfaces. The nature of the chemisorption site of methanethiol on a surface can be probed directly by TOF-SARS since by judicious choice of beam incidence and scattering angles, it is possible to probe down to the metallic substrate. It is generally believed that chemisorption occurs at a threefold site in which the adsorbate is centered above an equilateral triangle formed by three first-layer atoms. There are, however, two different threefold sites on {111} surfaces, i.e., the fcc site, which is directly above a third-layer atom and the hexagonal-close-packed (hcp) site, which is directly above a second-layer atom. TOF-SARS, coupled with classical ion trajectory simulations,[29] has recently shown[28] that CH_3SH is chemisorbed on Pt{111} by bonding of the S atom to a fcc threefold site at room temperature. At elevated temperatures, both the S and C atoms are bonded to the Pt surface at fcc and hcp threefold sites, respectively. Second, TOF-SARS has short-range structure sensitivity, i.e., it samples the ordered regions of the surface on a length scale of <10 Å. These ordered regions produce anisotropic scattering and recoiling features that contain compositional and structural information. The disordered regions and defects produce isotropic scattering and recoiling features that are observed as a continuous background in the angular scans. For example, the structure of crystalline paraffin films[30] and benzene[31] chemisorbed on single crystal metal surfaces have been deciphered by TOF-SARS. Third, the ability to directly detect hydrogen with high sensitivity allows study of the nature of the surface hydrogen, its involvement in the surface structure, and the degree of free rotation of the methyl end groups on the surface. The main limitations in studying SAMs terminated in other end groups are the limited mass resolution and the sensitivity of fluorinated moieties to radiation damage. Fourth, since this is a real-space technique, interpretation of the data in terms of model structures is straightforward, and the data can be simulated directly using classical ion trajectory calculations. More detailed comparisons to other techniques can be found elsewhere.[27,32]

The paper is organized as follows. Section II briefly describes the experimental and computational methods used in the study. Section III provides some structural considerations that are helpful for presentation and interpretation of the experimental and simulated results. The experimental results are presented in Sec. IV, first for the clean underlying Au{111} substrate and then for the three different SAMs. The simulations of the angular scans are presented in Sec. V along with the models used in the calculations. The results of the experiments and simulations are discussed in Sec. VI and the conclusions are summarized in Sec. VII.

II. METHODS AND MATERIALS

TOF-SARS was used for surface elemental analysis and structural characterization. Details of the technique have been described elsewhere.[27] Briefly, a pulsed noble gas ion beam irradiates the sample surface in an ultrahigh vacuum (UHV) chamber, and TOF spectra of the scattered and recoiled ions plus fast neutrals are measured. The primary 4 keV beam employed herein was Ne^+ for scattering from the Au substrate atoms and Ar^+ for recoiling of H, C, and F atoms. The ion pulse width was ~ 50 ns, the pulse repetition rate was 30 kHz, the average beam current was 1 nA/cm^2, and the TOF drift region was 90 cm long. The Ar scattering and H, C, and F recoiling intensities were calculated as the integrated intensity in 0.3 μs windows centered under the respective peaks following background subtraction. The angular notation is defined as follows: α is the beam incident angle relative to the surface; δ is the crystal azimuthal angle; θ is the scattering and recoiling angle.

Classical ion trajectory simulations were carried out by means of the three-dimensional scattering and recoiling imaging code (SARIC) developed in this laboratory. SARIC is based on the binary collision approximation, uses screened Coulomb potentials to describe the interactions between atoms, and includes both out-of-plane and multiple scattering. Details of the simulation have been published elsewhere.[29]

Hexadecanethiol (C_{16}) and heptadecanol were purchased from Aldrich Chemical Co. and used as received. Heptadecanethiol (C_{17}) was synthesized from heptadecanol using standard methods. 16,16,16-Trifluorohexadecanethiol (FC_{16}) was synthesized using an established procedure.[33] The polished {111} Au single-crystal surface was cleaned by repeated cycles of 0.5 keV Ar^+ sputtering and annealing to 550 °C in the UHV chamber. Annealing was accomplished by electron bombardment heating from behind the crystal. The surface was considered clean and well ordered when no impurity peaks were observed in the TOF-SARS spectra and the low energy electron diffraction (LEED) image exhibited sharp spots in a hexagonal pattern. The SAMs were prepared *ex situ* by immersing the gold substrate into 1 mM solutions of the alkanethiols in ethanol for periods of 24 h. Following reintroduction into the vacuum system, no further treatments were performed, since sputtering would have damaged the monolayer and annealing would have likely desorbed it, at least partially. The chamber was baked at a low temperature ($\sim$50 °C) for several days upon insertion of each new sample. The major limitation of the experiment is the sample degradation under ion bombardment. Even though TOF-SARS uses a low flux, pulsed ion beam, these organic molecules are extremely sensitive to the impinging keV ions. Recoil events can damage a molecule, manifested as dehydrogenation in case of H recoil or cleavage of C–C bonds in case of C recoil. Introduction of these types of defects is essentially irreversible since the defective structure cannot be corrected by annealing as in metal and semiconductor samples. LEED measurements were not attempted on the SAMs due to the well known high sensitivity of these films to electron beam damage. Furthermore, LEED patterns[19–21] of SAMs are available in the literature.

The total ion dose required for acquisition of a single

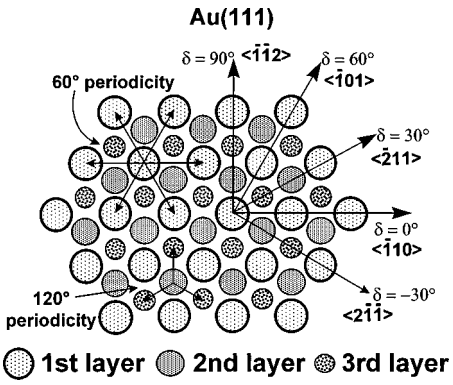

FIG. 1. Plan view of the ideal bulk-terminated Au{111} surface illustrating the azimuthal angle δ assignments and the sixfold and threefold symmetry of the first- and second-layer atoms, respectively.

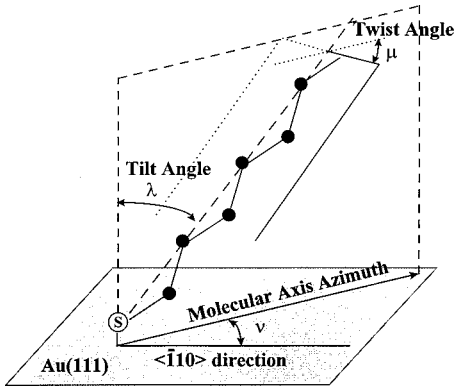

FIG. 2. Drawing of an alkanethiol chain defining the tilt angle of the molecular chain with respect to the surface normal (λ), the molecular axis azimuth (ν), and twist angle (μ).

TOF-SARS spectrum is $\sim 10^{11}$ ions/cm^2. The total ion dose after completion of an azimuthal scan on a fresh sample is $\sim 10^{13}$ ions/cm^2 and produces no observable degradation of the sample surface. However, sample degradation in the form of loss of some of the surface hydrogen was observed after performing such scans several times (typically four to five times) on a single sample. Therefore, the accumulated total ion dose where degradation was first noticed was $\sim 5 \times 10^{13}$ ions/cm^2, which can be compared with the surface carbon density of $\sim 4 \times 10^{14}$ atoms/cm^2. At this stage, no anisotropy of the scattered ion intensity can be measured, which indicates that the surface structure is already heavily disturbed. Further irradiation leads to an increase of the Ar multiple scattering peak from Au. This indicates that some ions can reach the substrate through the defective, sputtered SAM layer. A sharp Au scattering peak eventually appears at the final stage of degradation. All data, presented herein were collected in the range of low ion doses ($< 5 \times 10^{13}$ ions/cm^2) in order to avoid the complications of sample degradation.

III. STRUCTURAL CONSIDERATIONS

It is helpful to use structural models in order to aid in the presentation and discussion of the TOF-SARS experimental results and SARIC simulations. Such models are presented in this section. The proposed model for the SAMs is derived from the experimental and simulated data, as will be detailed in the ensuing sections.

One of the objectives of this study is to relate the structure of the SAMs to that of the Au{111} substrate, i.e., relating the Au crystallographic azimuthal directions to the nearest-neighbor and next-nearest-neighbor directions of the SAMs. In order to accomplish this, after TOF-SARS measurements had been made on a SAM, the film was removed from the surface by sputtering and annealing without moving the Au substrate. The azimuthal features of the Au were then measured, allowing direct relation of these Au features to the previously measured SAM features. The first-layer Au atoms exhibit 60° periodicity, whereas the subsurface layers exhibit 120° periodicity, as shown in Fig. 1. If the incident ion beam scatters along the 30° direction ($\langle 211 \rangle$ azimuth) or along the 90° direction ($\langle 112 \rangle$ azimuth), the second- and third-layer atoms are accessible to the beam at different incident angles α. This can be observed in Fig. 1 from the drawing of the atoms in the plane perpendicular to the {111} surface along the 30° $\langle 211 \rangle$ azimuth and along the 90° $\langle 112 \rangle$ azimuth.

Each molecular chain was allowed three degrees of freedom as shown in Fig. 2: (i) the tilt angle of the molecular chain with respect to the surface normal λ, (ii) the molecular axis azimuth ν, i.e., the angle between the projection of the molecular axis onto the Au{111} plane and the Au$\langle 110 \rangle$ azimuth, which is the Au nearest-neighbor direction, and (iii) the twist angle μ, defined by the angle made by the chain plane and the plane perpendicular to the surface containing the chain axis. SAMs are composed of an ordered assembly of such oriented molecules. Since keV ions scatter from atomic cores, i.e., the nucleus plus core electrons, whose radii are <0.2 Å, an ''ion's eye view'' of a SAM surface is a rather open structure, as shown in Fig. 3.

IV. EXPERIMENT RESULTS

A. Time-of-flight spectra

A typical TOF spectrum from the clean Au surface is shown in Fig. 4. The peak is identified by using the simple binary collision approximation to determine the scattering and recoiling energies and corresponding flight times for the various atomic collisions involved. The spectrum of clean Au exhibits a single sharp, intense peak for scattering from Au atoms, i.e., Au(s), which is centered at 7.0 μs. A broad, low intensity Ar multiple scattering peak, i.e., Au(ms), is observed at ~ 7.7 μs. There is no evidence of contaminants in this spectrum.

Typical TOF spectra from the C_{16}, C_{17}, and FC_{16} SAM-covered Au surfaces are shown in Figs. 5(a), 5(b), and 5(c), respectively. The spectra from the hydrocarbon SAM-covered surfaces exhibit peaks due to recoil of H at 5.1 and C at 6.3 μs, i.e., H(r) and C(r). The spectrum from the fluorocarbon SAM-covered surface exhibits a peak due to recoil of F atoms, i.e., F(r), at 7.2 μs in addition to H(r) and C(r). The FC_{16} molecule differs from the C_{16} molecule by replacement of the terminal methyl group by a trifluoromethyl group. This leads to a decrease of the H(r) peak in the TOF-SARS spectrum of Fig. 5(c) by about 30% as compared

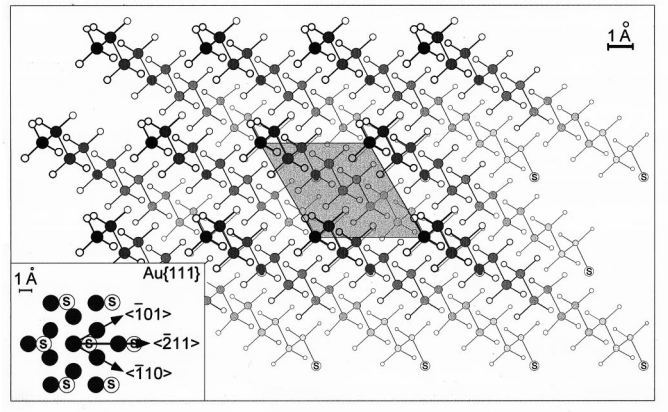

FIG. 3. Proposed ''ion's eye view'' model for the $CH_3(CH_2)_{15}SH$ SAM on Au{111}. The methyl C atoms at the surface are represented by solid black circles. The methylene C atoms of the molecular chains are represented by progressively smaller circles of lighter shades of gray with descending depth below the surface. The H atoms are represented by small open circles. The S atoms at the Au surface are labeled as such. Due to the inclination angle of the chains, the cores of the upper 12 C atoms of each chain are directly exposed to the surface normal. The outline of the $(\sqrt{3}\times\sqrt{3})R30°$ unit cell is indicated. This ''ion's eye view'' of the surface exhibits a regular array of sloping cavities of width ~5.0, length ~8.7, and depth ~12 Å within each unit cell. The inset shows the azimuthal orientation of the Au{111} structure with respect to that of the SAM unit cell. Note the different length scales used to represent the SAM and the Au structures.

to Fig. 5(a), which gives a good estimate of the fraction of the hydrogen recoil signal H(r) resulting from the terminating moieties.

The sharp scattering peak of Au(s) is not observed on the SAM-covered surfaces because the Ar atoms do not penetrate through the 16 or 17 layer carbon chains down to the Au substrate. This result shows that the SAMs form continuous films that fully cover the Au substrate. No sharp Ar scattering peak is observed from the SAMs themselves because the $\theta=50°$ scattering angle used in the experiment is far above the critical angles for single scattering of Ar from light atoms such as H, C, and F. The Ar multiple scattering feature becomes more distinct as the scattering angle is lowered. For example, at $\theta=40°$, the broad, monotonically decreasing intensity feature in the region 7–12 μs of Fig. 5(d)

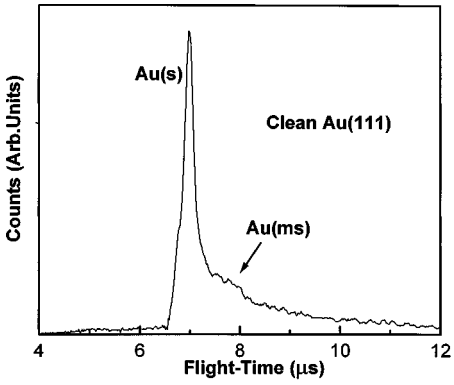

FIG. 4. TOF-SARS spectrum of 4 keV Ar scattering from a clean Au{111} surface. Au(s)=quasisingle scattering of Ar from Au; Au(ms)=multiple scattering of Ar from Au; incident angle $\alpha=22°$; scattering and recoiling angle $\theta=50°$.

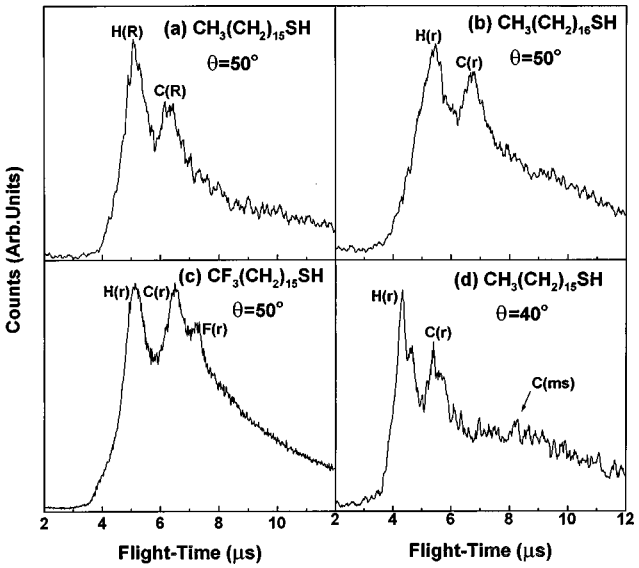

FIG. 5. TOF-SARS spectra of 4 keV Ar scattering and recoiling from self-assembled monolayers on a Au{111} surface. (a) $CH_3(CH_2)_{15}SH$ at $\theta=50°$; (b) $CH_3(CH_2)_{16}SH$ at $\theta=50°$; (c) $CF_3(CH_2)_{15}SH$ at $\theta=50°$; (d) $CH_3(CH_2)_{15}SH$ at $\theta=40°$. θ is the scattering and recoiling angle and the incident angle is $\alpha=22°$.

is due to Ar multiple scattering from the C atoms, i.e., C(ms). Since the critical angle[34] for Ar single scattering from C atoms in the classical limit is $\theta=\sin^{-1}(M_C/M_{Ar})=17°$, the scattered Ar atoms observed in this region for $\theta=40°$ must have each undergone at least three binary collisions.

The radiation damage effects observed for the C_{16} sample are shown in Fig. 6. The relative H(r) and C(r) peak intensities decrease due to loss of hydrogen and carbon and the relative C(ms) intensity increases with increasing ion dose due to damage and the consequent disorder of the films. The Au(s) peak becomes visible at a dose of $\sim 10^{15}$ ions/cm^2, indicating that portions of the SAM have been sputtered away and the ion beam has direct access to the Au substrate.

B. Identification of the Au{111} azimuthal directions

1. Incident angle α scans

Information on the subsurface structure along planes perpendicular to the surface can be obtained[35] by measuring scattering or recoiling intensities as a function of the incident angle α along different azimuthal directions δ. At grazing α, all atoms lie within the shadow cones of their preceding neighbors. As α is increased, the impact parameter required for scattering or recoiling into θ becomes accessible and a sharp increase in the scattered or recoiled intensity is observed due to focusing of ions at the edges of the shadowing and blocking cones. This critical incident angle α_c observed at lowest α corresponds to the angle at which first-layer atoms move out of the shadowing and blocking cones of their first-layer neighbors. Subsequent critical incident angles α_c observed at higher α correspond to the angles at which subsurface-layer atoms move out of the shadowing and

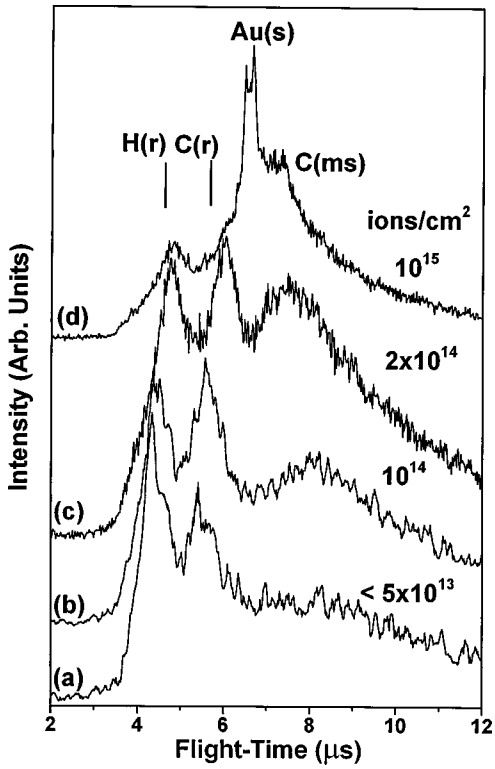

FIG. 6. TOF-SARS spectra of 4 keV Ar scattering and recoiling from a C_{16} SAM on Au{111} at $\theta=40$ and $\alpha=20°$ taken after different ion irradiation doses: (a) $<5\times10^{13}$ ions/cm^2, (b) $\sim1\times10^{14}$ ions/cm^2, (c) $\sim2\times10^{14}$ ions/cm^2, and (d) $\sim1\times10^{15}$ ions/cm^2.

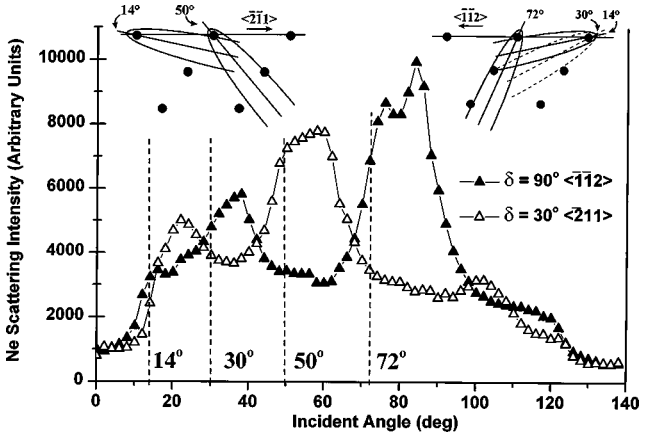

FIG. 7. Incident angle α scans of 4 keV Ne scattering intensity Au(s) along two azimuthal directions $\delta=30$ and 90° on the clean Au{111} surface. The positions of the critical incident angles α_c, as determined by a simple shadow cone analysis, are denoted by dashed lines. A simple shadow cone analysis of the critical incident angles α_c expected for 4 keV Ne scattering along these two azimuths is shown as insets above the plots. These insets represent planes that are perpendicular to the {111} surface and contain the 30 and 90° azimuths. Bulk interatomic spacings were used for these simulations.

blocking cones of atoms in layers nearer to the surface. The positions of the α_c's provide a direct measure of the interatomic spacings as shown elsewhere.[35]

The crystallographic azimuthal directions of the Au{111} surface can be determined by measuring incident angle α scans along the $\delta=30$ and 90° directions. TOF spectra similar to those for clean Au in Fig. 4 were obtained and the intensity of the scattering peak was plotted as a function of α as shown in Fig. 7. The critical incident angle α_c is measured at the position corresponding to 50% of the peak height after background subtraction. Along the $\delta=90°$ direction, only two peaks are observed corresponding to two α_c's, whereas along the $\delta=30°$ direction, three peaks are observed corresponding to three α_c's. In order to interpret these α scans, the shape of the shadow cone for 4 keV Ne scattering from an Au atom was calculated. This shadow cone shape can be used to obtain a simple and quick identification of the α_c's as follows. As shown in Fig. 7, for $\delta=30°$ the first $\alpha_c=14°$ corresponds to focusing by first-layer atoms onto their first-layer neighbors and the second $\alpha_c=50°$ corresponds to focusing by first-layer atoms onto their second-layer neighbors; this identifies the $\delta=30°$ direction as the $\langle211\rangle$ azimuth. For the $\delta=90°$ direction, the three α_c's observed are as follows. The first $\alpha_c=14°$ corresponds to focusing by first-layer atoms onto their first-layer neighbors. The second $\alpha_c=30°$ corresponds to focusing by first-layer atoms onto their second-nearest neighbors located in the second-layer. The third $\alpha_c=72°$ corresponds to focusing by first-layer atoms onto the subsurface rows whose atoms are aligned along this α and δ direction. The high intensity of this peak is a result of the many scattering centers accessible to the beam at this angle. This identifies the $\delta=90°$ direction as the $\langle112\rangle$ azimuth.

2. Azimuthal angle δ scans

The surface periodicities can be determined[36] by monitoring the scattering or recoiling intensities as a function of the crystal azimuthal angle δ. The minima are coincident with low-index azimuths where the interatomic spacings are short and the surface atoms are inside of the shadowing and blocking cones cast by their aligned nearest neighbors, resulting in low intensities. As δ is scanned, the atoms move out of the shadow cones along the intermediate δ directions where the interatomic spacings are long, resulting in an increase in intensity. The widths of the minima are related to the interatomic spacings along the particular direction. Wide, deep minima are expected from short interatomic spacings because of the larger degree of rotation about δ required for atoms to emerge from neighboring shadows.

TOF spectra similar to those for clean Au (Fig. 4) were obtained and the intensity of the scattering peak was plotted as a function of δ, as shown in Fig. 8. The δ scan for the Au surface exhibits well-defined 120° periodicity with deep, wide minima along the $\delta=0$ and 60° directions due to the short first-layer interatomic spacings along these azimuths. The minimum along $\delta=30°$ is narrow and very shallow due to the long first-layer interatomic spacings. The minima along $\delta=-30$ and 90° are narrow due to the long first-layer interatomic spacings along these azimuths and different from those of the $\delta=30°$ direction due to the different second- and third-layer atomic arrangement. The incident angle of $\alpha=14°$ used in this δ scan is high enough to allow the beam to sample the second-layer atoms, thereby providing a distinction between the $\delta=30$ and the $\delta=-30$ and 90° azi-

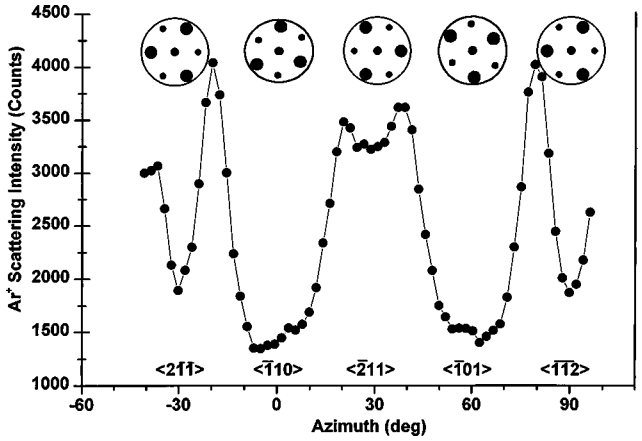

FIG. 8. Azimuthal angle δ scan of 4 keV Ne scattering intensity Au(s) from the clean Au{111} surface. Incident angle $\alpha=14$; scattering angle $\theta=50°$. The orientations of the LEED patterns that correspond to the azimuthal orientations of the sample at the positions of the observed minima are indicated on the figure.

muths. Schematic LEED patterns are shown above the respective minima, illustrating the positions of the diffraction spots obtained for the different crystal alignments. Each 30° azimuthal rotation corresponds to rotation of the LEED pattern by 30°. The 120° repetition period of the LEED pattern is in agreement with the periodicity obtained from TOF-SARS.

C. Azimuthal structure of the SAMs

Azimuthal scans were carried out on the SAMs in order to gain information on their surface azimuthal periodicity, atomic structure, degree of order, and their relationship to the underlying Au structure. The TOF-SARS technique has been widely used for surface structural studies of single-crystal materials, including mostly metal, semiconductor, and metal oxide surfaces.[36] There are at least five major differences between these materials and SAMs that must be considered for ion scattering. First, the SAMs have organized structures,[5] but the flexible hydrocarbon chains do not possess the rigid order of single crystals. Second, the light H and C atoms have large vibrational amplitudes and rotational motions that tend to broaden the TOF spectra and the α and δ scans. Third, the light H, C, and F atoms are most efficiently detected as recoils since the Ar scattering cross section from C is small and the critical angles for single scattering of heavier projectile atoms are low. Also, the recoiling cross sections themselves are small. Fourth, the SAMs are made up of individual chains of organic molecules that are chemically reactive. Fifth, ion-induced surface damage cannot be annealed as in metal and semiconductor crystals. In order to obtain good azimuthal scans, one has to find a compromise between a sufficient ion dose to obtain good statistics without causing degradation of the surface. Surface degradation limits the number of azimuthal scans that can be performed on a single sample.

1. The $CH_3(CH_2)_{15}SH/Au\{111\}$ SAM

A clear azimuthal anisotropy with a 60° periodicity was found for the C_{16} samples from both the H(r) and C(r) signals as shown in Fig. 9(a). The $\delta=0°$ azimuth refers to the $\langle 110\rangle$ direction of the Au{111} substrate (Fig. 1). The H(r) signal exhibits maxima every 60° which are shifted by 30° with respect to the nearest-neighbor directions of the Au substrate (Figs. 1 and 3). The C(r) signal exhibits minima every 60° which coincide with the H(r) maxima. We reproduced this result several times on three different C_{16} samples. The same pattern was consistently observed, although the features weakened every time that the measurement was repeated on a single sample, showing evidence of surface degradation under ion irradiation. The C(r) maxima correspond to the azimuths with the largest C–C interatomic spacings (next-nearest-neighbor C atom directions) and the minima correspond to the azimuths where C(r) is severely blocked due to short C–C interatomic spacings (nearest-neighbor C atom directions). H(r) is primarily blocked by the heavier C atoms, therefore the H(r) minima correspond to directions of alignment of C and H atoms. No azimuthal features were observed at very low incident angles, i.e., less than 15°, which indicates that the surface disorder and/or roughness was sufficient to obliterate the azimuthal sensitivity for such grazing trajectories.

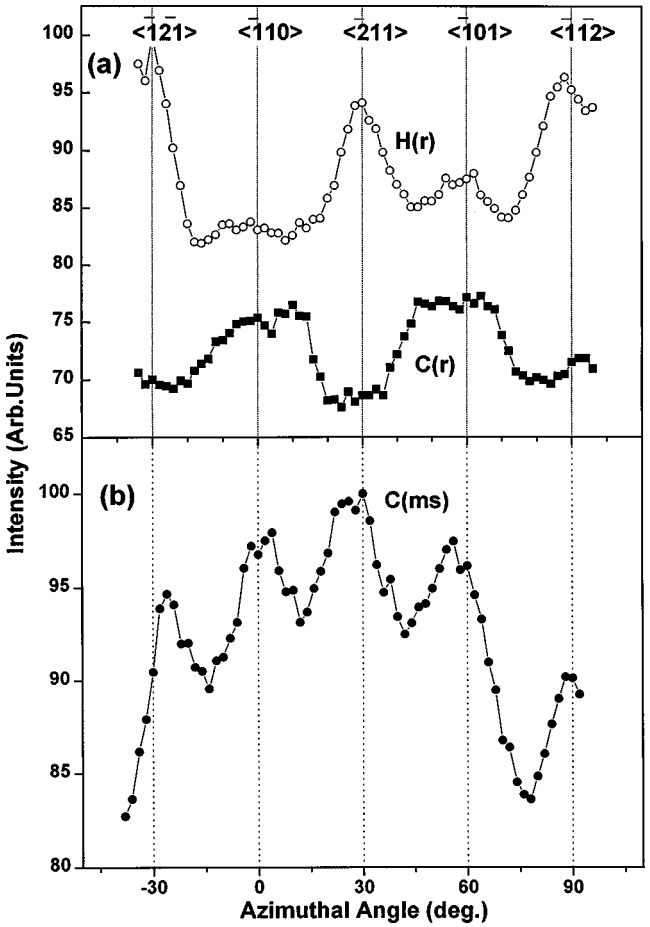

FIG. 9. Azimuthal angle δ scans using 4 keV Ar^+ ions for (a) H and C recoiling intensities, H(r) and C(r), from the C_{16} surface with $\theta=50°$ and (b) Ar multiple scattering intensity from carbon, C(ms), on the C_{16} surface with $\theta=40°$. Incident angle $\alpha=22°$. The azimuthal reference $\delta=0°$ corresponds to the Au{111} substrate $\langle 110\rangle$ direction.

Figure 9(b) shows the azimuthal anisotropy for Ar scat-

tering with $\theta = 40°$ from C atoms, i.e., the broad C(ms) feature from Fig. 5(d). The azimuthal scan exhibits maxima every 30°, coinciding with both the nearest-neighbor C atom and next nearest-neighbor C atom directions of the C_{16} SAM. Unlike recoiling, multiple scattering collisions have the highest probability of occurring along the azimuthal directions of highest atomic density. This result is consistent with the recoiling data, showing that near-surface organization exists in the form of well-defined atomic rows of the molecular adsorbates.

Interpreting the azimuthal scans from the C_{16} samples presented in Fig. 9 is not straightforward and requires computer simulation. Nevertheless, a few important qualitative conclusions may be drawn at this stage. First, the extent of the intensity variations with the azimuthal rotation (Fig. 9) is small (~10%) as compared to typical scans from single-crystal metal surfaces (~70%), such as the Au{111} substrate (Fig. 8). This indicates that, as expected, the surface is sufficiently organized to produce azimuthal anisotropy, but does not possess the rigid ordering of metallic single crystals. Even if a perfect packing of the alkane chains is assumed, the wagging motions of such flexible molecular chains can impart large lateral and perpendicular displacements from the ideal lattice site positions. This disorder decreases the shadowing and blocking effects that produce the anisotropy in the δ scans. The second conclusion concerns the $C(r)$ minima of Fig. 9(a) which occur at 30° from the Au{111} nearest-neighbor directions. From simple shadowing and blocking arguments, a lower $C(r)$ intensity is expected along the SAMs nearest-neighbor directions, i.e., the directions of shortest C–C spacings. This is fully consistent with previous AFM[10] and LEED studies[19–21] that indicate a $(\sqrt{3}\times\sqrt{3})R30$ adsorption of alkanethiols on Au{111}. Since the alkane chains are believed to be tilted, there may be several domains coexisting at the surface. With an Au{111} surface, six equivalent tilting directions might be expected, which can lead to six different domains for the SAMs.

2. The $CH_3(CH_2)_{16}SH/Au\{111\}$ SAM

The C_{17} molecules differ from the C_{16} molecules by one additional methylene group in the chain. This is expected to modify the orientation of the end methyl groups at the surface.[5,37] The C_{17} samples were prepared and analyzed in exactly the same manner as the C_{16} samples, allowing a direct comparison. Surprisingly, the azimuthal scans of these C_{17} samples displayed very poor features. Representative scans comparable to those of Fig. 9(a) and obtained under exactly the same conditions are shown in Fig. 10(a). Note that the intensity scale is expanded relative to Fig. 9(a). The $H(r)$ signal still shows weak maxima near $\delta = -30$ and 30° with possibly an intermediate maximum near $\delta = 10$. The $C(r)$ signal shows an irregular variation, with weak minima near −30, 30, and 90°. The overall intensities are much weaker than those observed for the C_{16} molecules and are only slightly larger than the statistical fluctuations of the measurement, which are of the order of a few percent. However, these azimuthal variations are not totally random. The measurement was reproduced on three different samples and the scans were always similar; this argues against the possibility of having defective samples. The anisotropy in the δ scans was noticed only at the very beginning of ion irradiation. The data very quickly became isotropic by the second or third δ scan, implying that any further disorder produced at the surface makes structural measurements impossible. It appears that, although the C_{16} and C_{17} SAMs differ by only one methylene group, the extent of their surface azimuthal periodicity as determined by TOF-SARS and their sensitivity to irradiation by keV ions are markedly different.

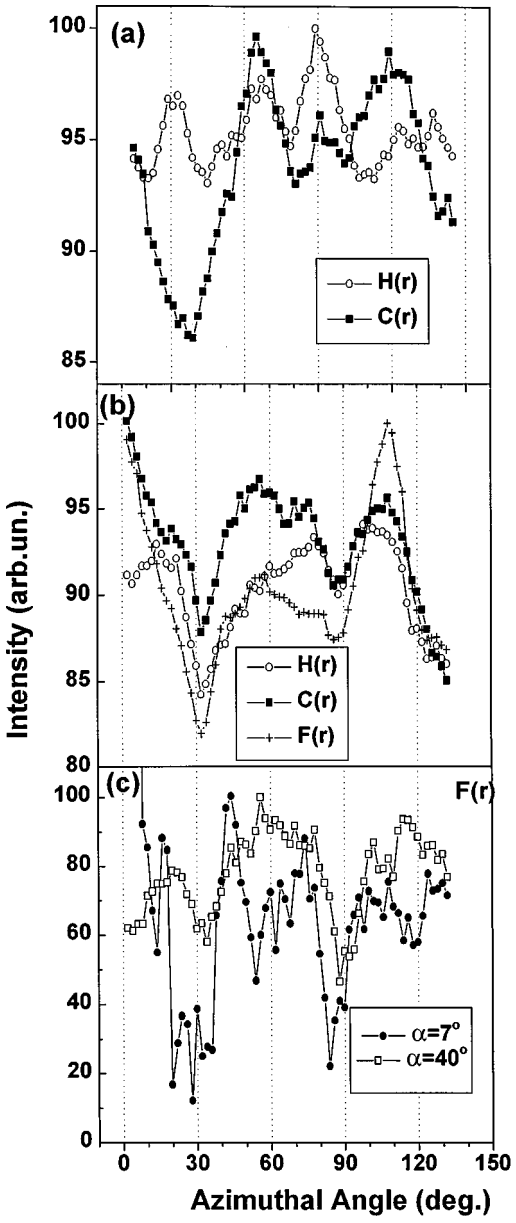

FIG. 10. Azimuthal angle δ scans of H, C, and F recoiling intensities, $H(r)$, $C(r)$, and $F(r)$, using 4 keV Ar^+ ions from: (a) the C_{17} surface with $\theta = 50$ and $\alpha = 22°$; (b) the FC_{16} surface with $\theta = 50$ and $\alpha = 22°$; (c) the $F(r)$ intensity from the FC_{16} surface with $\theta = 50$ and $\alpha = 7$ and 40°. The azimuthal reference $\delta = 0°$ corresponds to the Au{111} substrate ⟨110⟩ direction.

3. The $CF_3(CH_2)_{15}SH/Au\{111\}$ SAM

The azimuthal scans in Fig. 10(b) obtained under the same conditions as the other two SAMs show some weak

variations of the H(r), C(r), and F(r) signals. These signals are lower along the 30 and 90° directions, which are the directions of the major orientations of the SAM molecular chains. The scans of Fig. 10(c), which were taken at grazing incidence ($\alpha=7°$) and grazing exit ($\beta=10°$) angles, also show weak minima for F(r) along these directions, but no variation was measured for H(r) and C(r). At such a grazing incidence, the ions will mainly probe the order of the topmost layer, i.e., the order of the CF_3 groups. The weak minima observed in Fig. 10(c) are a direct result of the surface order possessed by the CF_3 groups, i.e., these groups do not assume random orientations. The observed features indicate that the packing of the FC_{16} SAM is consistent with that of the hydrocarbon SAMs. Furthermore, this observation is consistent with previous AFM measurements[7] which detected similar packing structures of fully hydrogenated and trifluoromethyl terminated 13 carbon atom SAMs. Monolayers formed from fully fluorinated alkanethiols have been shown to possess an altogether different packing structure.[10]

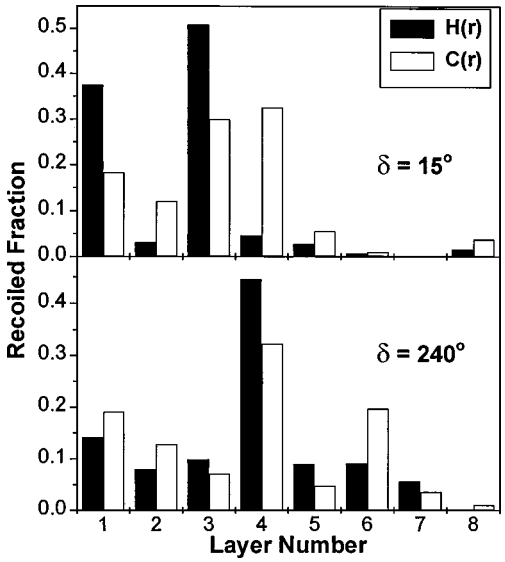

FIG. 11. Fraction of H and C atoms recoiled by 4 keV Ar^+ ions from the first through the eight atomic layers of the C_{16} SAM with the beam aligned along two different azimuthal directions $\delta=15$ and 240°. $\alpha=22$; $\theta=50°$.

V. CLASSICAL ION TRAJECTORY SIMULATIONS

Due to the complex nature of the surfaces of the SAMs, it was necessary to use classical ion trajectory simulations to relate the experimental data to the surface structure. SARIC was used for these simulations. The models tested were based on a hexagonal lattice of molecular chains as suggested by our azimuthal scan of Fig. 9 and by other structural studies[38] of SAMs. A lattice parameter of 4.995 Å, which is $\sqrt{3}$ times the Au{111} surface lattice parameter, was used and the molecules were arranged in a $(\sqrt{3}\times\sqrt{3})R30$ structure on the surface. Each molecular chain was allowed three degrees of freedom as shown in Fig. 2: the molecular tilt angle λ, the molecular axis azimuth ν, and the twist angle μ.

A. TOF-SARS sampling depth on SAM surfaces

The first important question that needs to be answered is the sampling depth in the ion scattering measurements. The keV ions scatter from atomic cores, i.e., the nucleus plus core electrons. Such atomic cores have radii of the order 0.1–0.2 Å. Therefore the ''ion's eye view'' of a $(\sqrt{3}\times\sqrt{3})R30°$ SAM surface structure is an open lattice, with a nearest-neighbor distance of ~5 Å, consisting of light atoms which do not scatter the Ar ions efficiently (Fig. 3). The ions are thus expected to substantially probe the subsurface methylene groups below the terminating CH_3 or CF_3 groups. The depth sensitivity of the scattering spectra was estimated by using a model consisting of hypothetical crystalline alkanethiol films of different chain lengths, starting from a single methyl group, i.e., SCH_3, on Au{111}. For each new CH_2 group added to the molecular chain, the amount of H(r) and C(r) detected in the simulation was recorded using incident, azimuthal, and scattering angles similar to those used in the experimental measurements. The difference between the recoiling yield for a chain with (n) C atoms and the yield for a longer chain with ($n+1$) C atoms, i.e., $(I_{n+1}-I_n)$, gives the amount of H(r) and C(r) generated from the additional subsurface ($n+1$)th-layer. The results of this calculation for two different azimuths are shown in Fig. 11. The atomic layer of origin of the recoils is strongly dependent on the beam azimuthal alignment. Most of the recoils originate from the first four atomic layers and no significant signal comes from below the seventh layer. The high recoil signal from the third and fourth layers is due to focusing of the incoming ions onto these layers by the SAM structure and subsequent scattering from these layers. This is a direct result of the ''ion's eye view'' of the open nature of the SAM structure as shown in Fig. 3. These simulations of the sampling depth show that C_{16} SAMs can be modeled by using alkyl chains having only eight carbon atoms.

The experimental spectra of the SAMs in Fig. 5 show no scattering peak from the Au substrate for a fresh sample. This has been tested by simulating a C_{16} layer on a Au{111} surface. The molecule was approximated by its carbon backbone without hydrogen, since hydrogen atoms do not produce any significant shadowing and blocking. The simulated TOF spectrum, shown in Fig. 12, does not exhibit any contribution from the Au substrate. The same simulation carried out with only a seven carbon alkyl chain, however, exhibits a scattering peak from the Au substrate. Clearly, the 4 keV Ar^+ ions are able to penetrate the seven atomic layers, where they are scattered from the Au substrate, and then traverse the seven atomic layers again in order to be detected. This measurement is consistent with the sampling depth simulations of Fig. 11.

B. Molecular chain configuration of the C_{16} SAM

A major question concerns the configuration of the molecular chains. Since there are three angles λ, μ, and ν involved in specifying the chain orientations, all possible permutations of the configurations of the chains could not be simulated. We have therefore selected a reasonable set of angles from those reported in previous studies[1,5,38] as a starting point. The simulation is actually even more complex since the individual chains have no symmetry. Although the

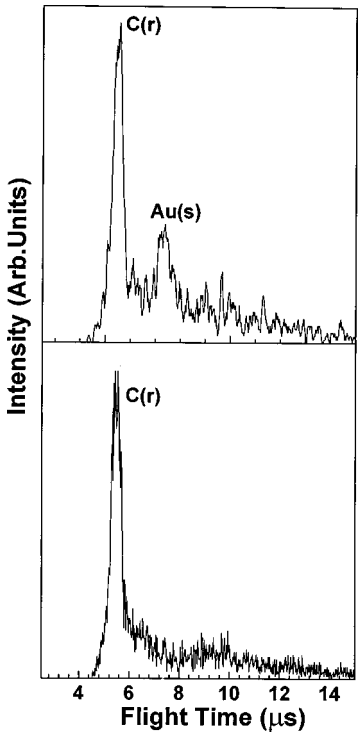

FIG. 12. Simulated TOF-SARS spectra for SAMs composed of molecular chains containing 7 carbon layers and 16 carbon layers. No hydrogen atoms were included in the chains. Primary ions 4 keV Ar^+; $\alpha=22$; $\theta=40°$.

surface lattice is hexagonal, a full azimuthal scan covering $\delta=360°$ is necessary for simulation. The results of these simulations do not exhibit any periodicity on a scale of less than 360°, in contrast to the 60° periodicity observed experimentally (Fig. 9). This is direct evidence for the coexistence of six equivalent domains on the surface, as the chains can assume six equivalent tilting directions on the Au{111} surface. Each of these domains is tilted by some multiple of 60° with respect to the others. This situation was simulated by first calculating the asymmetrical full $\delta=360°$ azimuthal scan representing a single domain. This single domain result was then shifted by 60° five different times to represent six different domains. Assuming that each of the domains has equal probability, the results of the six individual azimuthal scans were added. The final result is an azimuthal scan with a 60° periodicity.

It is generally agreed[1,5,38] that the molecular axis azimuth ν (Fig. 3) is aligned with the SAMs next-nearest-neighbor direction ($\nu=0°$), corresponding to the substrate's nearest-neighbor direction, with a tilting angle in the range[12,17,18,22–24] of $\lambda\sim27–37°$; calculations were performed for $\lambda=30$ and 35°. Calculations were also performed for two different molecular axis azimuths, $\nu=0$ and 30°. Only the 0° direction was found to provide agreement with the experimental data. The next step was to vary the twist angle μ. Three configurations were tested: (1) untwisted ($\mu=0°$), with the molecular plane perpendicular to the surface, (2) twisted by $\mu=55°$, which is a twist of the alkane crystalline phase, and (3) a fully twisted molecule ($\mu=90°$). The simulation using configuration number (2) with $\mu=55°$, shown in Fig. 13(a), was the only one that provided a

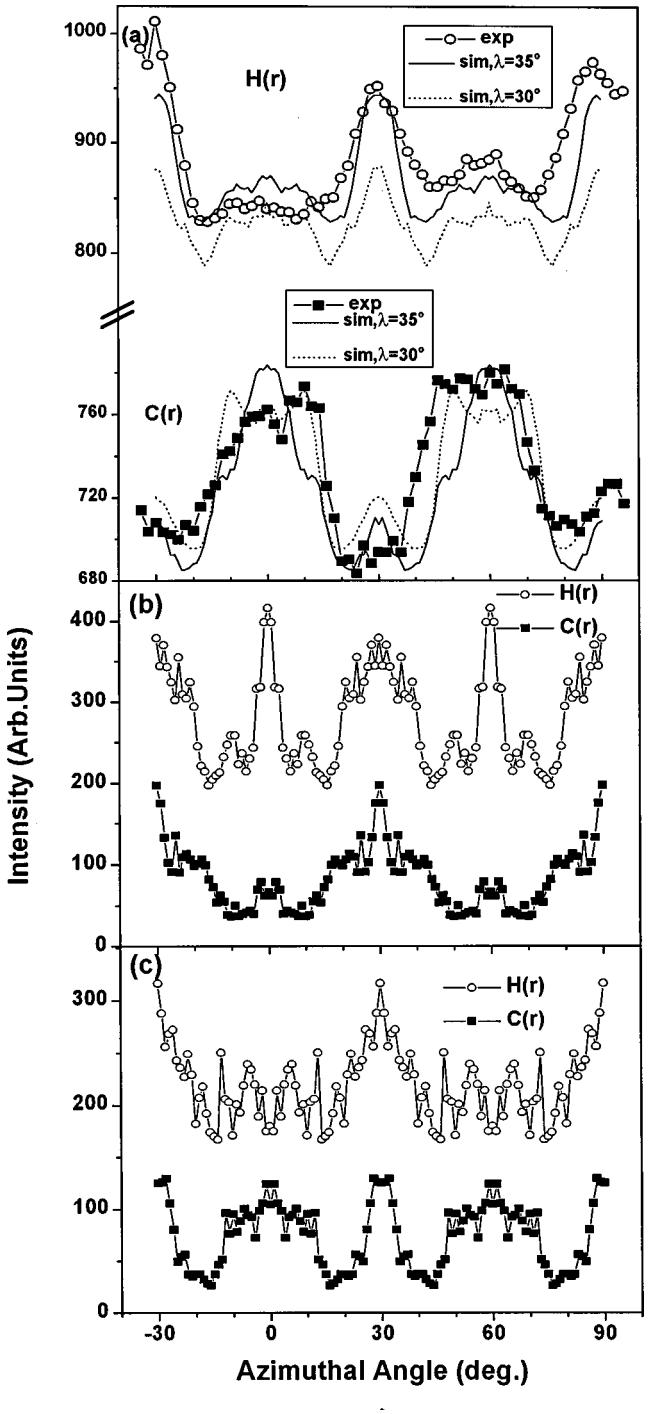

FIG. 13. SARIC simulations of the azimuthal angle δ scans of H(r) and C(r) from C_{16} SAMs using 4 keV Ar^+ ions. The angles defining the configurations were: (a) $\lambda=30$ and 35, $\nu=0$, $\mu=0°$; (b) $\lambda=35$, $\nu=0$, $\mu=55°$; (c) $\lambda=35$, $\nu=0$, $\mu=90°$. The experimental data from Fig. 9 are shown for comparison. $\alpha=22$; $\theta=50°$.

good match for the experimental data of Fig. 9(a). These final simulated scans were also obtained by mixing the two equivalent twist rotations, i.e., $\mu=55$ and $-55°$. Energetically a clockwise or a counterclockwise twist of the same amplitude are exactly equivalent and are equally likely to occur. Better agreement with the experimental data is obtained by using this assumption. The H(r) maxima along the nearest-neighbor directions are accurately reproduced in Fig.

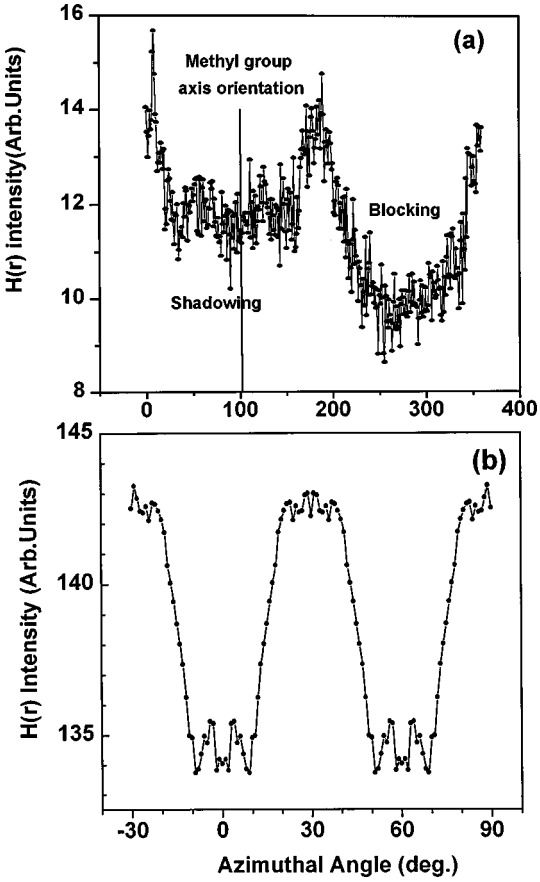

FIG. 14. SARIC simulations of azimuthal angle δ scans of H(r) from a methyl group tilted by 31° (a) in a single domain and (b) in six equivalent domains that are rotated by 60° from each other. $\alpha=22$; $\theta=50°$.

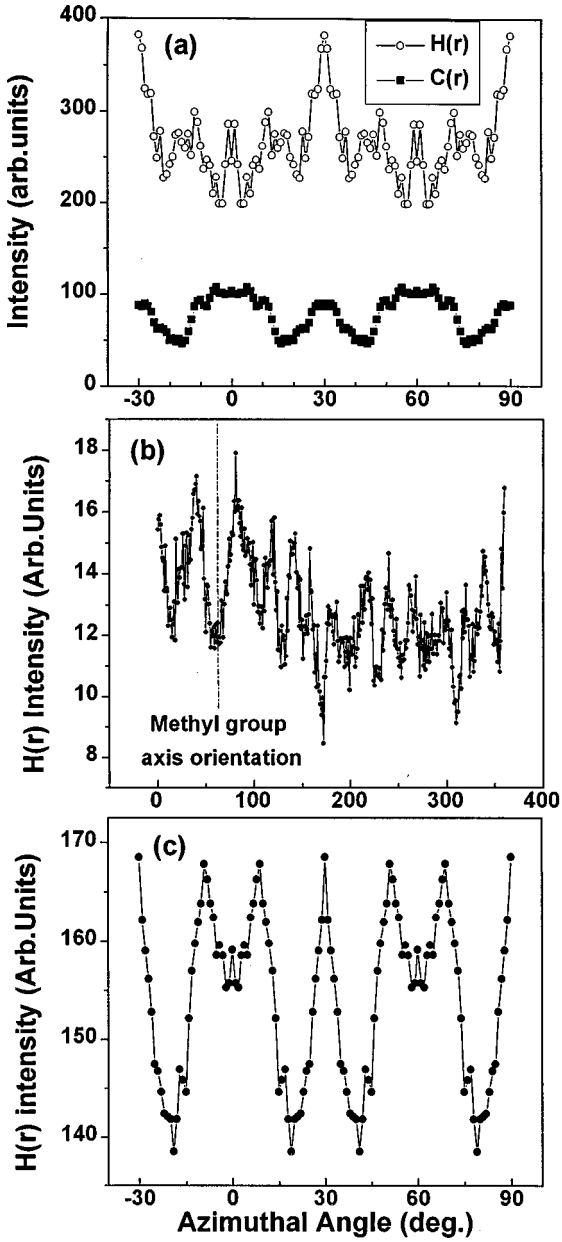

FIG. 15. SARIC simulations of azimuthal angle δ scans using 4 keV Ar^+ ions: (a) H(r) and C(r) from a C_{17} chain with tilt angle $\lambda=35$, molecular azimuth direction $\nu=0$, and twist angle $\mu=55°$. (b) H(r) from a methyl group tilted by 61° in a single domain. (c) H(r) from a methyl group tilted by 61° in six equivalent domains that are rotated by 60° from each other. $\alpha=22$; $\theta=50°$.

13(a), and even the small secondary maxima at 0 and 60° are confirmed. The C(r) scan is also well reproduced, with wide minima coinciding with the H(r) maxima and wide maxima centered around $\delta=0$ and 60°. The simulation with $\lambda=35°$ provides slightly better agreement with the experimental data than the one with $\lambda=30°$.

The simulation using configuration number (1), i.e., the untwisted model, is shown in Fig. 13(b); it provides poor agreement with the experimental scan. It shows abnormally high H(r) intensity at 0 and 60° and incorrect variations of the C(r) intensity. The simulation using configuration number (3), i.e., the fully twisted case, is shown in Fig. 13(c); it is also unrealistic, exhibiting high C(r) maxima where minima are observed experimentally in Fig. 9(a).

C. Configuration of the methyl groups at the surface of the C_{16} SAM

The positions of the three hydrogen atoms of the methyl groups were arbitrarily fixed in the above simulations. The exact configuration of these methyl groups at the surface and the possibility of their free rotation about the C–C axis should be distinguishable, since these methyl groups contribute to about one-third of the total H(r) signal (Fig. 5). If the C_3 axis of the methyl group is perpendicular to the surface, there would be no anisotropy in the H(r) scans, whether the group is fixed or freely rotating, because the H atoms would be above the surface and out of the range of the C atom shadowing and blocking cones. If the axis is tilted with respect to the surface, there would be strong shadowing and blocking of the H atoms lying in the lower part of the methyl group near the surface by the C atoms since the C–H bond length is only 1.07 Å. According to the previous model, the methyl group in a C_{16} chain is tilted by ~31° from the surface normal. In order to verify this, eight fixed methyl groups, each one rotated by 15° from the previous one to cover the 120° symmetry of the methyl group, were created for simulation. A complete $\delta=360°$ azimuthal scan was then calculated for each configuration. Finally, all of these scans were normalized over the number of incident projectiles and

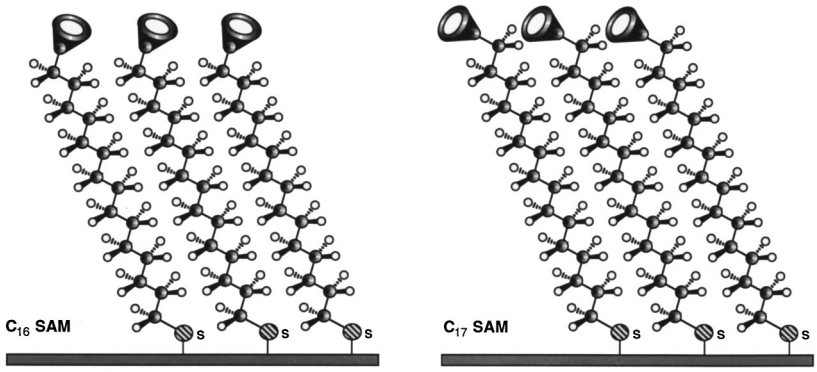

FIG. 16. Models of the C_{16} and C_{17} SAMs on Au showing the orientations of the ''ring'' of H atom density at the terminal methyl groups.

added, simulating the azimuthal scan of a freely rotating tilted methyl group and its corresponding ''ring'' of H atom density. As can be seen in Fig. 14(a), the H(r) scan from a methyl group tilted 31° is highly anisotropic. The intensity is lower in a wide sector around the tilt direction, i.e., $\delta \sim 97°$. This corresponds to shadowing of the lower part of the methyl H atom ''ring'' by the C atoms. Similarly, the intensity is lower in a wide sector around the direction opposite to the tilting direction, i.e., $\delta \sim 277°$, due to blocking of H(r) from the lower part of the ring by the C atoms. The recoiling intensity is highest in two narrow sectors perpendicular to the tilt direction, i.e., 0 and 180°, because no efficient shadowing or blocking by the methyl C atoms occurs in these directions. Finally, it is necessary to consider the existence of six domains at the surface, which means six different tilting directions. The final scan, obtained by adding the scans from the six domains, is given in Fig. 14(b). Clearly, a freely rotating methyl group at the surface whose axis is tilted by 31° from the normal leads to H(r) maxima corresponding to the experimental observation of Fig. 9(a). Such simulations for methyl groups with fixed positions of the H atoms do not provide azimuthal features in agreement with Fig. 9(a).

The simulated total amount of H(r) recoiled from the methyl groups accounts for ~30% of the amount of H(r) recoiled from the entire chain, which is consistent with the estimation made from the FC_{16} spectrum of Fig. 5(c).

D. Simulations of the C_{17} SAM

In order to simulate the C_{17} SAM, a molecular chain containing nine carbon atoms, $CH_3(CH_2)_8SH$, was constructed. The molecular configuration was assumed to remain the same, i.e., $\lambda = 35°$, $\mu = \pm 55$, and $\nu = 0°$. The major difference from the C_{16} SAM is that the end methyl group of the C_{17} SAM is tilted by the larger angle of 61° with respect to the surface normal. As previously, six domains are assumed, with two equivalent twists. The calculated azimuthal scans for C(r) and H(r) are shown in Fig. 15(a). No comparison is shown with the experimental data of Fig. 10(a) since the observed experimental variations were extremely weak. The C(r) anisotropy is clearly much less pronounced for this odd chain case than for the even chain case of Figs. 9, 13, and 14, and no minimum is observed along the SAMs nearest-neighbor directions $\delta = 0$ and 60°; instead, maxima are calculated along these two directions. This dramatic decrease of the C(r) anisotropy agrees with the weak azimuthal pattern observed experimentally in Fig. 10(a). The intensity changes fall below the statistical fluctuations of the method and no clear reproducible δ scan was obtained. The reason for such weak azimuthal features from the C_{17} SAM is that, due to the large tilt angle of the methyl groups, the methyl C atoms and the adjacent second-layer methylene C atoms exist in planes that are separated by only ~0.6 Å. Since the C atoms in both of these planes are approximately equally accessible for recoiling, and they occupy different azimuthal positions, the resulting azimuthal features are indistinct. The simulated H(r) azimuthal variations, however, display maxima along the SAMs nearest-neighbor directions [Fig. 15(a)], although they are slightly less pronounced than in the even chain case. These maxima were measured experimentally [Fig. 10(a)], although they were not as clear as in the C_{16} case. Other less intense maxima were observed at $\delta = 30$ and 90° that are not suggested by the simulation.

The freely rotating methyl group was also simulated for the C_{17} case by following the same procedure as before. Since the group is highly tilted, the azimuthal scan is now very different from that of the even chain situation as shown in Fig. 15(b). The intensity fluctuates irregularly, with a deep minimum along the tilting direction. The fluctuations are partly due to the discrete nature of the calculation and would vanish if a larger number of configurations were included in the simulation. When considering the usual six different domains, the simulation produces pronounced H(r) azimuthal features, with maxima every 30° as shown in Fig. 15(c). This simulation provides a reasonable match for the experimental δ scan of Fig. 10(a), which also exhibits maxima at approximately every 30°. The minor minima observed in the simulation of Fig. 15(c) at 0 and 30° are not observed in the experimental scan of Fig. 10(a). These results indicate that most of the H(r) anisotropy comes from the surface methyl groups.

E. Simulations of the FC_{16} SAM

Extensive simulations were not carried out for FC_{16} since the experimental data of Figs. 10(b) and 10(c) exhibited such weak azimuthal variations. We did, however, perform simulations for fixed and freely rotating CF_3 groups. Angular parameters similar to those used in Sec. V C for C_{16}

were used for CF_3, including a CF_3 group tilt angle of 31°. Such simulations with fixed positions of the F atoms in the CF_3 groups exhibited a high degree of anisotropy, inconsistent with the weak variations of Figs. 10(b) and 10(c). This anisotropy could only be dampened by assuming a freely rotating CF_3 group as for the CH_3 group of Sec. V C.

VI. DISCUSSION

Some outstanding questions concerning SAMs can be addressed from the experimental and simulated results presented here. Interpretation of these results provides an understanding of some of the structural features characteristic of SAMs on gold. Unlike the highly ordered single-crystal samples to which the TOF-SARS technique is usually applied, the SAMs consist of an assembly of flexible *molecules*. Models of the C_{16} and C_{17} SAMs are shown in Fig. 16. A schematic drawing of the model proposed for the C_{16} SAMs is given in Fig. 3 as an ''ion's eye view'' of the structure, i.e., the positions of the atomic cores as experienced by the incoming keV ions. As indicated from this figure, due to the tilt angle of the SAMs, the cores of the C atoms are directly exposed to the surface normal down to the twelfth layer of C atoms from the surface. It is therefore possible for a keV ion incident at the surface normal to make direct scattering collisions with sub-end group C and H atoms as deep as the twelfth layer. Such deep layer collisions are not very probable in our case because of the low incident beam angle α and scattering angle θ used in the measurements. Indeed, as shown in Fig. 11, most of the recoiled atoms come from the outermost four atomic layers.

The results of the azimuthal alignment measurements of Secs. IV B and C show that the molecular chains are tilted along the SAMs next-nearest-neighbor directions, which is the nearest-neighbor direction, i.e., the $\langle 110 \rangle$ azimuth, of the Au{111} substrate. Our recent study[28] of methanethiol on Pt{111} showed that this simplest prototypical alkanethiol chemisorbs above the fcc threefold site. This site is consistent with azimuthal alignments found herein, suggesting that these longer chain alkanethiols also chemisorb above the fcc sites on Au{111}. Forthcoming studies of methanethiol adsorbed on Au{111} will further explore this issue.

Two quasiindependent systems must be considered in a structural analysis of these monolayer assemblies: the individual alkyl chains and the lattice formed by an assemblage of these chains. The shadowing and blocking effects that take place within these two quasi-independent structural systems are different. Intramolecular effects occur between the closely spaced atoms, 1.54 for C–C and 1.08 Å for C–H, of a single molecule. Intermolecular effects occur between atoms of the different molecules which are separated by at least 5 Å. The nature of the order within each system is also different. The atoms building up the individual molecular chains are almost fixed due to the strong C–H and C–C bonds, although phenomena such as *gauche* defects must be considered. In contrast, the molecular chain units are flexible near the surface, allowing both lateral ''wagging'' motion (and hence a quasidisordering of the hexagonal lattice) as well as perpendicular motion.

These different degrees of order pose major limitations for the structural analysis and the simulations. Only isotropic displacements of the target atoms can be varied in the SARIC program, which is suitable for simulating the thermal vibrations in a monoatomic crystal. In the SAMs, there are small vibrational amplitudes of the atoms making up the chains that are coupled to the larger translational motions of the flexible chains themselves. The simulations herein were performed with isotropic vibrational atomic displacements of 0.1 Å, which is equivalent to freezing the molecular translational motions, but allowing some small bond length variations in the form of vibrational amplitudes inside the chains. The flexibility of the molecular chains near the surface is therefore neglected, which limits the accuracy of the simulations. Introducing larger vibrational amplitudes would be even less realistic, since this would ignore the influence of the chemical bonds of the molecules as well as the van der Waals stabilization associated with interchain interactions.[5]

In the ion scattering experiments detailed herein, the ions reach the surface at an incidence angle $\alpha = 22°$ and produce recoils of C and H atoms from the methyl groups and from several methylene groups further below the surface. The trajectories of the H(r) recoils from the methyl groups will not interact with the neighboring molecular chains since they leave at an exit angle of 28°. These recoils will then carry the signature of the methyl group azimuthal anisotropy. The trajectories of the H(r) recoils from the methylene groups below the surface, however, will be close to the atoms of neighboring molecular chains and will interact with them. Due to the flexibility of these chains, the anisotropy of these subsurface recoils will be attenuated in the experiments and will be overestimated in the simulations. A careful examination of some of the H(r) trajectories from the methylene groups shows strong focusing effects by C atoms of neighboring chains. These effects will be strongly dependent on the movements or translational motion of the molecular chains away from their ideal lattice positions. Therefore, the azimuthal anisotropy of the H(r) from the surface methyl groups, which accounts for about 30% of the total observed H(r) intensity, is not affected by this lattice disorder. As a result, the simulations will exaggerate the anisotropy due to the molecular chain organization, but will provide reliable anisotropies for the topmost atoms of the SAMs. The H(r) anisotropy produced by the surface methyl groups should, therefore, account for much more than 30% of the total observed variation.

Some experimental facts support this assumption. First, although the simulations reproduce the main features of the azimuthal scans, the simulated amplitude of the variations is two to three times larger than expected experimental amplitudes, as a result of the surface disorder. This is particularly prominent at grazing incidence or exit angles where only weak anisotropy, if any, was measured. For such conditions, the scattering and recoiling intensities become very sensitive to the surface corrugation due to the tilt angle of the molecular chains. Second, the C(r) anisotropy was always found to be more sensitive to the radiation induced damage than the H(r) anisotropy, and in many cases the H(r) anisotropy could still be observed when the C(r) signal showed no dis-

tinct features. Trajectory analyses show that almost all the $C(r)$ anisotropic features are produced by shadowing and blocking effects between neighboring molecular chains. The $C(r)$ intensity from the topmost carbon layer was found to be largely isotropic. Hence the $C(r)$ intensity variations reflect the degree of organization of the molecular chains of the SAMs, and these variations are attenuated as the structure degrades and becomes more disordered. Third, for both the C_{16} and C_{17} SAMs, the best agreement between the experimental and simulated data is obtained with a freely rotating methyl group.

When comparing the C_{16} and C_{17} SAMs, we would expect there to be little difference in the order or crystallinity of the two films. Furthermore, due to the fact that the C_{17} SAMs possess an additional methylene group (and thus additional van der Waals stabilization[5]), we might expect these SAMs to exhibit more order than the C_{16} SAMs. However, the C_{16} azimuthal scans exhibit sharp features while the C_{17} azimuthal scans exhibit weak features. The weak features of the C_{17} SAM are believed to be caused by the large tilt angle of its methyl groups ($\sim$61°), which results in a spacing of only $\sim$0.6 Å between the first two C layers as described in Sec. V D. Furthermore, while the FC_{16} SAMs possess well ordered structure [as judged by surface infrared (IR) spectroscopy[39]], these SAMs exhibit the weakest azimuthal features of all. These results reveal a basic limitation of TOF-SARS: since it is a real-space technique, it cannot discern the structures of systems with large unit cells or systems with many inequivalent atoms in a unit cell. The short first–second-layer C spacing with C atoms at different azimuthal positions in the C_{17} SAM and the heavy F atoms of the tilted CF_3 group at different heights above the surface in the FC_{16} SAM present structures which are currently at the limitations of the TOF-SARS technique.

One intriguing observation is that the C_{16} SAMs appear to damage less readily than the C_{17} SAMs upon exposure to keV ions. Since the TOF-SARS technique samples only the outermost portion of the films, these observations might suggest a relationship between damage susceptibility and the orientation of the terminal methyl C–H or C–C bonds. If this interpretation proves to be correct, terminal group orientation might become an important consideration in applications where SAMs are used as protective coatings.[40] The FC_{16} SAM exhibits a high susceptibility to damage by the keV ions; however, this is not surprising since fluorocarbons are generally[41] sensitive to radiation damage.

VII. SUMMARY

The final proposed model for the SAMs derived from our ion scattering and trajectory simulation studies can be summarized as follows. The alkyl chains chemisorb with the S atoms situated above the fcc threefold sites of the Au{111} surface to form a continuous film with a $(\sqrt{3}\times\sqrt{3})R30°$ structure that fully covers the Au surface. These films are sufficiently organized to produce azimuthal anisotropy in ion scattering measurements. For most of the conditions used herein, the scattered and recoiled signals originate from the outermost five–six atomic layers. The molecular axis azimuth ($\nu=0°$) of the SAMs is directed along the Au substrate nearest-neighbor direction $\langle\bar{1}10\rangle$, which is the SAMs next-nearest-neighbor direction. A tilt angle of $\sim$35° with respect to the surface normal is found to be consistent with the data. This tilt angle results in direct exposure of the C atomic cores to the surface normal down to the twelfth atomic layer. The molecular planes are also twisted by $\sim$55° with respect to a plane normal to the surface. Six domains, corresponding to the six tilt directions of the molecular chains, coexist and two equivalent twist orientations ($\pm$55°) are consistent with the data. The results do not indicate whether these two orientations can be found in one domain, as previously suggested,[12,13] or whether each domain has only one twist orientation. For even chains, the methyl group is tilted with respect to the normal by $\sim$31°; for odd chains, the methyl group is tilted with respect to the normal by $\sim$61°. Both types of methyl groups are freely rotating. These differences in the methyl tilt angle lead to dramatic changes in the anisotropic patterns of the ion scattering azimuthal δ scans due to the extreme surface sensitivity of the technique; the C_{16} SAM exhibits sharp anisotropic δ patterns while the C_{17} SAM exhibits weak anisotropy in the δ patterns. These weak patterns from the C_{17} SAM are most likely due to the short interlayer spacing between the first–second-layer C atoms resulting from the large tilt angle of the methyl groups. The C_{16} SAM is considerably more resistant to radiation damage from the incident Ar^+ beams than the C_{17} or the FC_{16} SAMs; the origin of these differences is not readily apparent. Azimuthal features were discernible from the data of the CF_3 terminated SAM at grazing incidence or exit angles, indicating that the CF_3 groups at the surface form an ordered structure. The observed features indicate that the packing of the FC_{16} SAM is consistent with that of the hydrocarbon SAMs and that the CF_3 groups are freely rotating.

ACKNOWLEDGMENTS

This work was supported by the MRSEC Program of the National Science Foundation under award number DMR-9632667 and the National Science Foundation under Grant Nos CHE-9700665 and DMR-9700662.

[1] For a recent review, see A. Ulman, Chem. Rev. **96**, 1533 (1996).
[2] G. M. Whitesides and P. E. Laibinis, Langmuir **6**, 87 (1990).
[3] D. A. Hutt and G. J. Leggett, Langmuir **13**, 3055 (1997).
[4] A. N. Parikh and D. L. Allara, J. Chem. Phys. **96**, 927 (1992).
[5] P. E. Laibinis, G. M. Whitesides, D. L. Allara, Y.-T. Tao, A. N. Parikh, and R. G. Nuzzo, J. Am. Chem. Soc. **113**, 7152 (1991); R. G. Nuzzo, L. H. Dubois, and D. L. Allara, *ibid.* **112**, 558 (1990); L. H. Dubois, B. R. Zegarski, and R. G. Nuzzo, J. Chem. Phys. **98**, 678 (1993).
[6] L. Strong and G. M. Whitesides, Langmuir **4**, 546 (1988).
[7] H. I. Kim, T. Koini, T. R. Lee, and S. S. Perry, Langmuir **13**, 7192 (1997).
[8] H. Schonherr and G. J. Vancso, Langmuir **13**, 3769 (1997); H. Schonherr, F. J. B. Kremer, S. Kumar, J. A. Rego, H. Wolf, H. Ringsdorf, M. Jaschke, H.-J. Butt, and E. Bamberg, J. Am. Chem. Soc. **118**, 13,051 (1996).
[9] K. Hu and A. J. Bard, Langmuir **13**, 5114 (1997).
[10] G.-Y. Liu and M. Salmeron, Langmuir **10**, 367 (1994).
[11] J. Pan, N. Tao, and S. M. Lindsay, Langmuir **9**, 1556 (1993).
[12] E. Delamarche, B. Michel, Ch. Gerber, D. Anselmetti, H.-J. Guntherödt, H. Wolf, and H. Ringsdorf, Langmuir **10**, 2869 (1994).
[13] G. E. Poirier, Chem. Rev. **97**, 1117 (1997); G. E. Poirer and M. J. Tarlov, Langmuir **10**, 2853 (1994).
[14] K. C. Chan, T. Kim, J. K. Schoer, and R. M. Crooks, J. Am. Chem. Soc. **117**, 5875 (1995).
[15] O. Cavalleri, S. E. Gilbert, and K. Kern, Surf. Sci. **377**, 931 (1997).

[16] D. L. Patick, V. J. Cee, and T. P. Beebe, Jr., Science **265**, 231 (1994).
[17] N. Camillone, III, T. Y. B. Leung, and G. Scoles, Surf. Sci. **373**, 333 (1997); N. Camillone, III, C. E. D. Chidsey, G. Liu, and G. Scoles, J. Chem. Phys. **98**, 4234 (1993); N. Camillone, III, P. Eisenberger, T. Y. B. Leung, P. Schwartz, G. Scoles, G. E. Poirier, and M. J. Tarlov, *ibid.* **101**, 11,031 (1994); N. Camillone, III, C. E. D. Chidsey, G. Liu, and G. Scoles, *ibid.* **98**, 3503 (1993); N. Camillone, III, T. Y. B. Leung, P. Schwartz, P. Eisenberger, and G. Scoles, Langmuir **12**, 2737 (1996).
[18] P. Fenter, P. Eisenberger, and K. S. Liang, Phys. Rev. Lett. **70**, 2447 (1993); P. Fenter, A. Eberhardt, and P. Eisenberger, Science **266**, 1216 (1994); P. Fenter, P. Eisenberger, J. Li, N. Camillone, III, S. Bernasek, G. Scoles, T. A. Ramanarayanan, and K. S. Liang, Langmuir **7**, 2013 (1991).
[19] J. Baldwin, N. Schuhler, I. S. Butler, and M. P. Andrews, Langmuir **12**, 6389 (1996); M. A. Bryant and J. E. Pemberton, J. Am. Chem. Soc. **113**, 8284 (1991).
[20] B. Heinz and H. Morgner, Surf. Sci. **372**, 100 (1997).
[21] F. Balzer, R. Gerlach, G. Polanski, and H.-G. Rubahn, Chem. Phys. Lett. **274**, 145 (1997).
[22] H.-J. Himmel, Ch. Woll, R. Gerlach, G. Polanski, and H.-G. Rubahn, Langmuir **13**, 602 (1997).
[23] L. H. Dubois, B. R. Zegarski, and R. G. Nuzzo, J. Chem. Phys. **98**, 678 (1993).
[24] R. Bhatia and B. J. Garrison, Langmuir **13**, 4038 (1997).
[25] J. J. Gerdy and W. A. Goodard, III, J. Am. Chem. Soc. **118**, 3233 (1996).
[26] H. Morgner, Langmuir **13**, 3990 (1997).
[27] J. W. Rabalais, Science **250**, 521 (1990); O. Grizzi, M. Shi, H. Bu, and J. W. Rabalais, Rev. Sci. Instrum. **61**, 740 (1990).
[28] S. S. Kim, Y. Kim, L. Kim, T. R. Lee, S. S. Perry, and J. W. Rabalais, J. Chem. Phys. (in press).
[29] V. Bykov, C. Kim, M. M. Sung, K. J. Boyd, S. S. Todorov, and J. W. Rabalais, Nucl. Instrum. Methods Phys. Res. B **114**, 371 (1996); M. M. Sung, V. Bykov, A. Al-Bayati, C. Kim, S. S. Todorov, and J. W. Rabalais, Scanning Microsc. **9**, 321 (1995).
[30] P. Bertrand, H. Bu, and J. W. Rabalais, J. Phys. Chem. **97**, 13,788 (1993).
[31] H. Bu, P. Bertrand, and J. W. Rabalais, J. Chem. Phys. **98**, 5855 (1993).
[32] C. Kim, C. Höfner, A. Al-Bayati, and J. W. Rabalais, Rev. Sci. Instrum. **69**, 1676 (1998).
[33] M. Graupe, T. Koini, V. Y. Wang, G. M. Nassif, R. Colorado, Jr., R. J. Villazana, H. Dong, Y. F. Miura, O. E. Shmakova, and T. R. Lee, J. Fluorine Chem (in press).
[34] E. S. Parilis, L. M. Kishinevsky, N. Yu, L. Turaev, B. E. Baklitzky, F. F. Umarov, V. Kh. Verleger, S. L. Nizhnaya, and I. S. Bitensky, *Atomic Collisions on Solid Surfaces* (North-Holland, New York, 1993).
[35] J. W. Rabalais, CRC Crit. Rev. Solid State Mater. Sci. **14**, 319 (1988).
[36] M. Shi, Y. Wang, and J. W. Rabalais, Phys. Rev. B **48**, 1689 (1993); M. M. Sung, J. Ahn, V. Bykov, J. W. Rabalais, D. D. Koleske, and A. E. Wickenden, *ibid.* **54**, 14,652 (1996).
[37] Y.-T. Tao, J. Am. Chem. Soc. **115**, 4350 (1993); Y.-T. Tao, M.-T. Lee, and S.-C. Chang, *ibid.* **115**, 9547 (1993).
[38] *Characterization of Organic Thin Films*, edited by A. Ulman (Butterworth-Heinemann, Boston, 1995).
[39] Fourier-transform infrared (FTIR) spectroscopy shows that the degree of crystallinity of the methylene chains of C_{16} and FC_{16} SAMs is indistinguishable: M. Graupe, S. S. Perry, and T. R. Lee (unpublished results).
[40] See, for example: G. K. Jennings and P. E. Laibinis, J. Am. Chem. Soc. **119**, 5208 (1997); F. P. Zamborini, J. K. Campbell, and R. M. Crooks, Langmuir **14**, 640 (1998); J. E. Ritchie, C. A. Wells, J.-P. Zhou, J. Zhao, J. T. McDevitt, C. R. Ankrum, J. Luckner, and D. R. Kanis, J. Am. Chem. Soc. **120**, 2733 (1998).
[41] P. E. Laibinis, R. L. Graham, H. A. Biebuyck, and G. M. Whitesides, Science **254**, 981 (1991); J. Phys. Chem. **97**, 9456 (1993); T. J. Lenk, V. M. Hallmark, C. L. Hoffmann, J. F. Rabolt, D. G. Castner, C. Erdelen, and H. Ringsdorf, Langmuir **10**, 4610 (1994).